Proceedings of the Pakistan Academy of Sciences: A Physical and Computational Sciences 62(3): 235-246 (2025)

ISSN (Print): 2518-4245; ISSN (Online): 2518-4253
http://doi.org/10.53560/PPASA(62-3)702

Pakistan Academy of Sciences

Research Article

Synthesis, Characterization, and Adsorptive Performance of Ag-Doped ZnO Nanoparticles for Melanoidin Removal

Mehwish Qaseem[1], Saeed Ahmad[2], Muhammad Yasir Khan[1]*, Muhammad Wasim Akhtar[3], Muhammad Furqan Ali[1], Muhammad Saquib Ali[1], Shakeel Ahmed[1], Shahid Bhutto[4], and Mehwish Altaf[1]

[1]Department of Chemical Engineering, University of Karachi, Karachi, Pakistan
[2]Department of Chemical Skills, Yanbu Technical Institute, Yanbu, Saudi Arabia
[3]Department of Metallurgy & Material Engineering, Mehran University of Engineering and Technology, Jamshoro, Sindh, Pakistan
[4]Centre of Environmental Studies, Pakistan Council of Scientific & Industrial Research (PCSIR), Karachi Complex, Karachi, Pakistan

Abstract: Melanoidin, a complex polymer compound formed through Maillard reactions during fermentation, constitutes a significant fraction of distillery wastewater and cannot be treated using standard treatment methods. Silver doped zinc oxide nanoparticles (AgZnONPs) were synthesized, characterized, and used in this work as potential adsorbent to remediate melanoidin from aqueous solutions. The as-synthesized nanoparticles were evaluated using X-ray diffraction (XRD), UV-visible spectroscopy, field-emission scanning electron microscopy (FE-SEM) with energy-dispersive X-ray spectroscopy (EDX), and Fourier-transform infrared spectroscopy (FTIR). Adsorption experiments were performed under varying operational parameters, including solution pH, mass of adsorbent, initial melanoidin concentration, and time of contact. Under optimal conditions, pH 7, 0.5 g/L adsorbent, 200 mg/L of adsorbate concentration, and 90 min contact duration, a maximum removal efficiency of 92% was achieved. The enhanced adsorption performance aligns with the Langmuir isotherm approach, demonstrating monolayer adsorption with a 50 mg/g maximum adsorption capacity. It adheres to pseudo-second-order kinetics, providing strong evidence of chemisorption with a rate-limiting mechanism and predominant process. These results illustrate the potential of AgZnONPs as a robust and efficient adsorbent material for the treatment of melanoidin-rich distillery effluents.

Keywords: Melanoidin, Silver-doped Zinc Oxide, Adsorption, Nanoparticles, Wastewater Treatment, Kinetic Modelling.

1. INTRODUCTION

Melanoidin molecules pose a challenge to the distillery industry because of their color and complex nature. In addition to its high biological oxygen demand (BOD) and chemical oxygen demand (COD), the alcohol industry faces several challenges, as previously described by Lin *et al*. [1]. Melanoidin molecules produce this color by reacting with sugar polymers and amino acids via the Maillard reaction [2]. The dark brown color of wastewater creates serious problems for carrier water bodies because it reduces the concentration of dissolved oxygen in water [3]. These compounds may also accumulate in aquatic species, potentially affecting their general health, growth, metabolism, and reproduction [4]. When melanoidin-rich wastewater is disposed off on land, it can disturb the nutritional balance and microbial activity, which are essential for plant and soil health, hindering seed germination due to chemical toxicity and decreased soil alkalinity [5].

Received: July 2025; Revised: August 2025; Accepted: September 2025
* Corresponding Author: Muhammad Yasir Khan <myasir@uok.edu.pk>

Conventional treatment techniques, such as biological and chemical methods, are generally ineffective for melanoidin degradation because of their complex molecular structures and high stability [6-7]. Advanced oxidation processes, such as photocatalytic degradation, have demonstrated up to a 90% removal efficiency [8]. However, their large-scale industrial application is hampered by catalyst deactivation, limited activity under visible light, high energy demand, and challenges in catalyst recovery and reuse [9]. Advanced technologies can significantly enhance the physical, chemical, and biological properties of distillery wastewater, including melanoidin degradation [10]. Among the advanced technologies explored, adsorption has emerged as a highly effective and economically viable approach owing to its ease of use, low energy requirements, and capacity to eliminate a variety of organic contaminants, including color-imparting molecules [11]. The use of nanomaterial-based adsorbents has further enhanced the efficacy of the adsorption process because of their variable surface chemical composition, large area of surface and reactivity [12]. Zinc oxide (ZnO) is amongst the mostly utilized metal oxides (MOs) owing to its high surface area, convenient synthesis, cost-effectiveness, and environmental compatibility. Thus, it has been widely considered by researchers seeking exceptional optical, chemical, physical, and electrical properties to enhance manufacturing and technical applications [13]. Abdelfattah and El-Shamy showed that ZnO has superior adsorption, photocatalytic activity under ultraviolet light, and structural stability compared to other MOs, including titanium dioxide (TiO_2) and iron oxide (Fe_2O_3) [14]. Nevertheless, the broad bandgap of ZnO (3.2 eV) hinders its activity under visible light, limiting its practical application in wastewater treatment. To get through these restrictions, doping ZnO with metal ions, especially silver, is a commonly investigated methodology to enhance its optical, electrical, and adsorption qualities [15]. It has been demonstrated that adding Ag increases the surface reactivity and electron mobility, while also tuning the bandgap, both of which are essential for enhancing the photocatalytic and adsorption performances [16]. Prior research has shown that Ag-doped ZnO nanostructures are exceptionally effective in adsorbing and degrading a range of organic contaminants, including pigments, phenolic compounds, and pharmaceutical residues [17-19]. Despite these promising outcomes, few investigations have been conducted on the adsorptive elimination of melanoidin using Ag-doped ZnO nanostructures. Furthermore, published reports lack a thorough examination of crucial parameters like impact of solution pH, and comprehensive kinetic and equilibrium evaluations. These discrepancies highlight the need for systematic research to elucidate the adsorption behavior of AgZnONPs toward melanoidin and to provide a mechanistic understanding that can inform the development of effective treatment plans.

In this study, AgZnONPs were synthesized using a co-precipitation technique, and their adsorption performance was examined in melanoidin solution (MS). Moreover, to gain more insight into the fundamental adsorption principle and processes, adsorption data were simulated and validated using kinetic and isothermal models, as depicted in Figure 1.

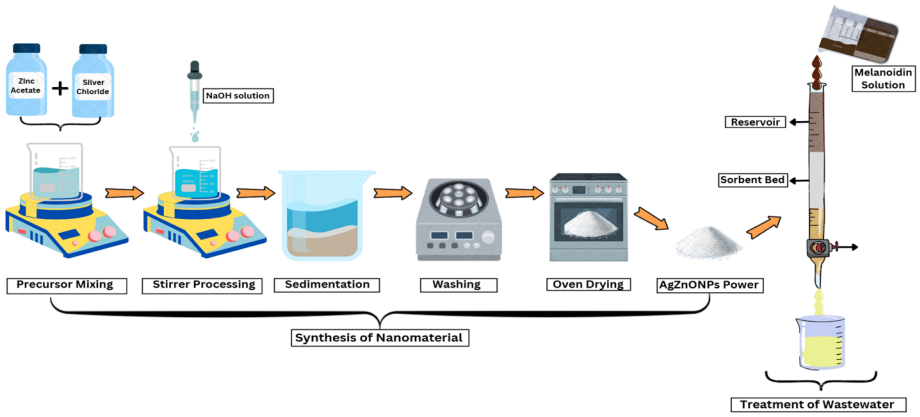

Fig. 1. Overall schematic representation of the synthesis of AgZnONPs and treatment of MS using the adsorption method.

2. MATERIALS AND METHODS

The reagents and chemicals used were extremely pure and of analytical quality. Zinc acetate (Zn $(CH_3CO_2)_2$), methanol (CH_3OH), sodium hydroxide (NaOH), Silver chloride (AgCl), glucose ($C_6H1_2O_6$), glycine ($C_2H_5NO_2$), and sodium bicarbonate ($NaHCO_3$) were bought from Sigma-Aldrich and utilized in their pure states. In this study, various analytical techniques were used to characterize the synthesized AgZnONPs. Crystallinity and phase composition were assessed using a Malvern Panalytical X'Pert3 spectrometer. TESCAN VEGA 4th generation instruments equipped with tungsten filament electron sources and EDS systems were used to examine the morphology and particle size of the AgZnONPs. To study the functional groups and characteristic bonds fourier-transform infrared spectroscopy (FTIR) analysis was executed using IR Prestige 21 (Shimadzu spectrophotometer). UV-visible spectroscopy was performed using a Shimadzu UV-1800 spectrometer.

2.1. Synthesis of Melanoidin Solution

The procedure discussed by Watcharenwong *et al*. [20] was executed to produce synthetic melanoidins. One hundred milliliters of distilled water were used to dissolve the reaction mixture containing 4500 mg of glucose, 1880 mg of glycine, and 420 mg of sodium carbonate. The prepared solution was oven dried for 7 h at 95 °C to promote melanoidin production. The substance was then cooled and freeze-dried for further examination. The molecular weight of the resulting melanoidin was calculated to be between 10,000 and 15,000 Da [21].

2.2. Synthesis of AgZnONPs

AgZnONPs were made via the co-precipitation technique. Zinc acetate was dissolved in 200 mL methanol (0.02 mol/L) and vigorously stirred at 500 rpm for 60 minutes at 55-60 °C. To add silver as a dopant, 17.48 mg of AgCl (1 atomic %) was added to the above solution. The separate solutions were made by mixing (3 g) $NaOH.H_2O$ then added to 50 mL of methanol, and the mixture was stirred for 60 min. Subsequently, 30 mL of NaOH/methanol solution was incorporated dropwise to the zinc acetate/methanol solution and agitated for 40 min. Subsequently, 200 mL of DI water was added to the solution and heated at 85 °C for 1 h with continuous mixing. The synthesized precipitate of AgZnONPs was centrifuged to obtain a colloid and repeatedly washed with methanol at least three times to remove residual oxidants. After centrifugation, the products were oven-dried and crushed in a mortar to obtain the AgZnONP powder. The reaction scheme for AgZnONP synthesis is shown in Figure 2.

2.3. Adsorption Experiments

The melanoidin removal from distillery wastewater was assessed through column adsorption experiments and the efficacy of AgZnONPs as an adsorbent. A column filled with AgZnONPs was used to pass MS at concentrations ranging from 50 to 500 mg/L, with an adsorbent dose from 0.1 to 1 g/L. Controlled flow conditions were employed in the column, and an effluent sample was collected at the outlet. Melanoidin concentrations in both the influent and effluent were measured using UV-UV-visible spectroscopy at a maximum wavelength of 291 nm. The removal percentage of melanoidin was calculated using the standard formula [22].

$$R\% = \frac{C_o - C_t}{C_o} \times 100$$

Where,

C_o is the initial concentration of MS (mg/L) at t = 0

C_t is the concentration of MS (mg/L) at time t (min).

2.4. Isotherms and Kinetics Studies

Kinetic experiments employing pseudo first-order and pseudo second-order models were conducted to elucidate the adsorption behavior of melanoidin on the produced nanoparticles [23]. These two models facilitate the assessment of adsorption rate

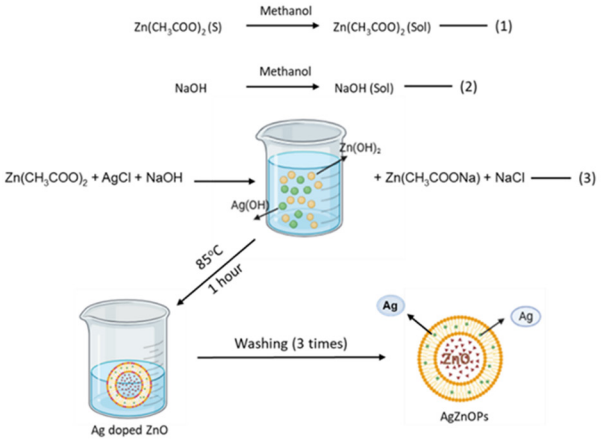

Fig. 2. Reaction scheme of synthesis of AgZnONPs.

and illustrate whether the process is influenced by chemical or physical interactions. Of these two, the model displaying the highest correlation with the experimental data revealed the primary mechanism. Furthermore, the Langmuir and Freundlich models were used in isothermal investigations to assess the adsorption equilibrium [24]. The Freundlich model takes multilayer adsorption on heterogeneous surfaces into account, while the Langmuir model assumes monolayer adsorption on a homogeneous surface. The adsorption mechanism, surface characteristics of the adsorbent, and process efficiency could be better understood when the data were fitted to these models.

3. RESULTS AND DISCUSSION

3.1. Structural Evaluation of AgZnONPs

The stimulated AgZnONPs were inspected using different analytical techniques. By using X-ray diffraction (XRD) analysis, the nanoparticles' crystalline structure and phase integrating were verified. while the FTIR spectra revealed the characteristic vibrations of both doped and undoped Zn-O bonds. Additionally, the SEM images showed particle size dispersion and morphology. Optical studies were performed using a UV-Vis spectrophotometer.

3.1.1. SEM analysis of AgZnONPs

SEM analysis was carried out to examine the structural traits and morphological characteristics of the synthesized AgZnONPs. Figure 3(a) shows that the cylindrical structures were shaped, confirming the presence of nanoparticles. In Figure 3(b), a similar view of the AgZnONPs is presented at a magnification of 25 K, providing a more detailed structural view than that in Figure 3(a) at a magnification of 5 k [25]. Both images demonstrated a compact structure and good grain size. Figure 3(c) shows a detailed elemental analysis of the AgZnONPs using energy-dispersive X-ray spectroscopy (EDX) analysis. The distinct peaks related to Ag, Zn, and O suggest that Ag was effectively integrated into the ZnO crystal structure [26]. The elemental maps of the AgZnONP samples were analyzed separately. The four highlighted elements, Zn, O, C, and Ag, are shown in Figure. 4.

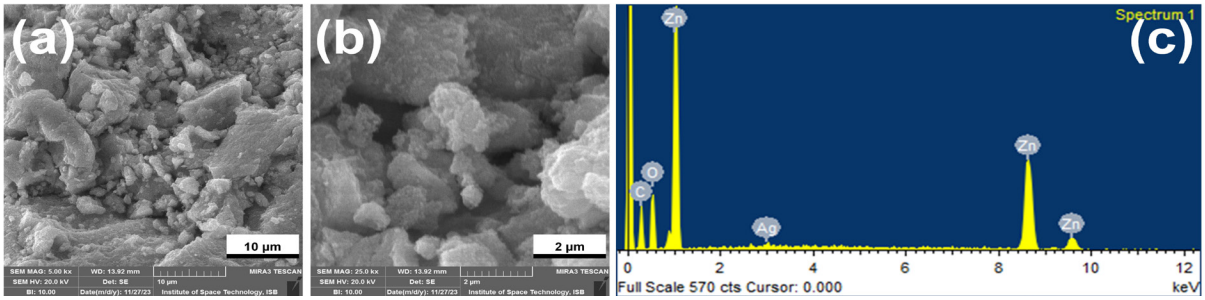

Fig. 3. FESEM images of AgZnONPs: (a) with top view at 5 K magnification, (b) top view at 25 K magnification, and (c) EDX analysis of AgZnONPs.

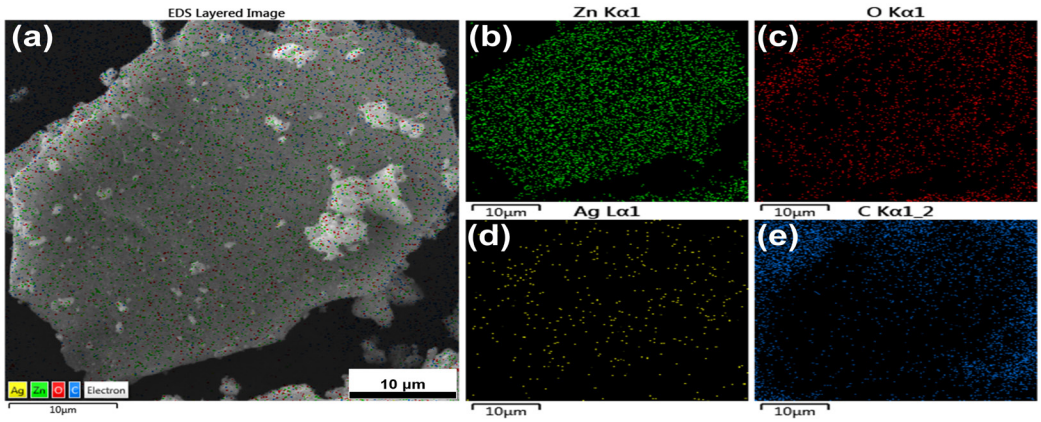

Fig. 4. FESEM images with (a) overall elemental mapping of AgZnONPs, (b) zinc h**ighlighted in green, (c) oxygen** highlighted in red, (d) Ag highlighted in yellow, and (e) carbon highlighted in blue.

3.1.2. X-ray Diffraction analysis of AgZnOPs

The XRD spectra of AgZnONP powder was obtained to confirm its structural properties. The XRD images reveal pure ZnO and AgZnONP diffraction peaks, as shown in Figure 5. The peaks ideally align with the hexagonal/wurtzite structure characterized by the space group P63mc (JCPDS No. 00-036-1451) [27]. It is evident that the 2θ values at 31.6°, 34.3°, and 36.1°, which represent the crystal planes (100), (101), and (101), respectively, make up the pattern of pure ZnO. In contrast, the diffraction peaks for AgZnONPs exhibited at 2θ = 31.7°, 34.4°, and 36.2°, corresponding to the change compared to undoped ZnO nanoparticles (ZnONPs) [28]. A prominent shift and higher values of the diffraction peaks of AgZnONPs are clearly visible in the figure, verifying the structural alteration in AgZnONPs as Ag+ ions are integrated into the ZnO Crystal lattice.

3.1.3. UV-VIS Spectroscopy of undoped ZnONPs and AgZnOPs

Figure 6 displays the UV-visible absorption spectra of the undoped AgZnOPs (red line) and ZnONPs (black line). The absorption edge of the undoped ZnONPs appeared at 396 nm with a lower intensity than that of the AgZnONPs at 411 nm. In the visible spectrum, silver doping increases the absorption intensity, accompanied by a noticeable increase in surface plasmon resonance (SPR), which is explained by the surface plasmon resonance (SPR) effect produced by silver nanoparticles [29]. The electronic band structure is changed and a red shift is indicated by the bandgap energy decreasing from 3.12 eV for undoped ZnONPs to 3.07 eV for AgZnONPs [30]. The effective integration of Ag into the matrix of ZnO was confirmed by the increase in optical absorption and change in bandgap energy.

3.1.4. FTIR of undoped ZnONPs and AgZnONPs

The undoped ZnONPs and AgZnONPs' FTIR spectra were captured in order to investigate the functional groups, vibrational modes, and bonding characteristics of the samples. Both materials exhibited distinctive absorption bands in the FTIR spectra, as shown in Figure 7, with significant variations observed upon silver doping. The

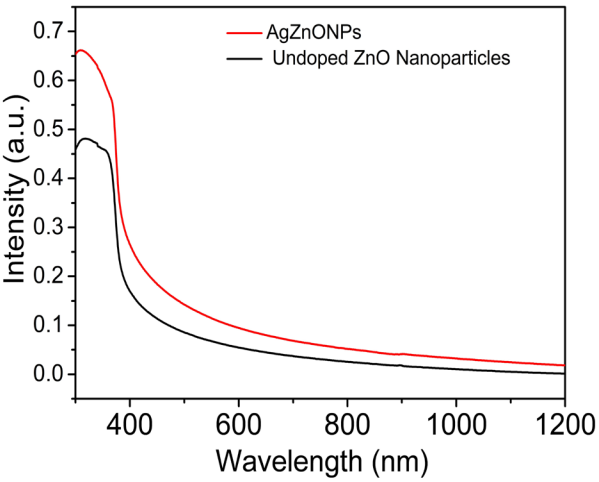

Fig. 6. UV-visible absorption spectrum of undoped ZnONPs and AgZnONPs.

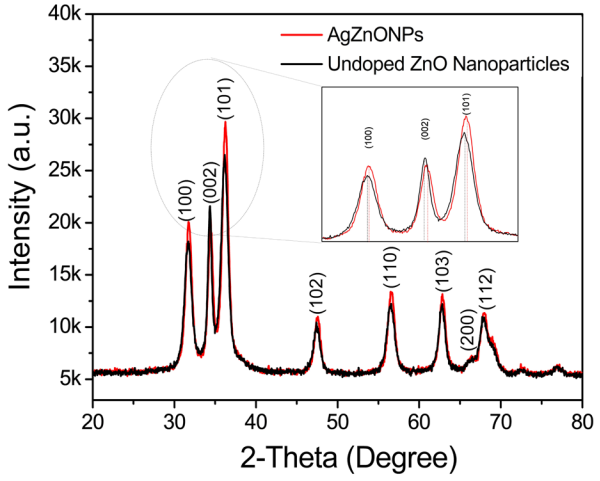

Fig. 5. XRD analysis of AgZnONPs (inset: higher magnification results of the main peaks).

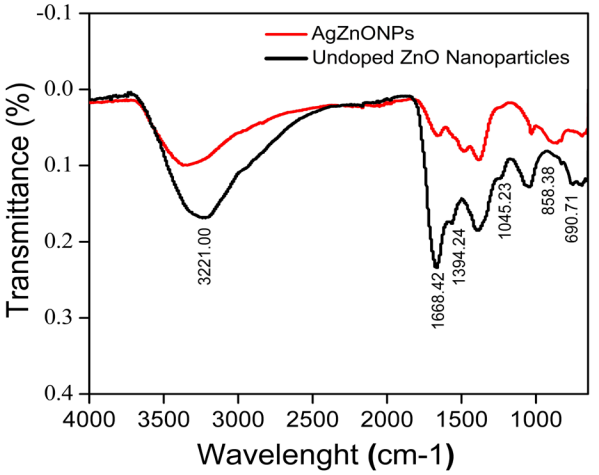

Fig. 7. FTIR spectra of undoped ZnONPs and AgZnONPs.

presence of surface-adsorbed moisture or hydroxyl groups is likely the cause of the broad absorption bands observed in both spectra at around 3000-3600 cm^{-1} and 1600 cm^{-1}, respectively. These bands were attributed to vibrations caused by O-H stretching and H-O-H bending. Additionally, both samples depict bands at about 1394 cm^{-1} and 1045 cm^{-1}, which are tentatively attributed to C-O stretching vibrations that may be caused by adsorbed ambient CO_2 [31]. The distinctive stretching vibration of the Zn-O lattice in undoped ZnO was detected at 690.71 cm^{-1}. The metal-oxide bond (ZnO) is associated with a band between 400 and 750 cm^{-1} [32-34]. The peaks in the Ag-doped ZnO spectrum are slightly moved to a lower wavenumber (688.69 cm^{-1}), suggesting that the addition of Ag ions has caused a little expansion of the ZnO lattice or a change in the strength of the Zn-O bond [35, 36]. Most prominently, the FTIR spectrum of Ag-doped ZnO shows a novel absorption peak at 858.38 cm^{-1} that is absent from the undoped ZnO spectrum. This new peak was ascribed to the stretching vibration of Ag inclusion [37].

3.2. Adsorption Studies

Adsorption performance tests are crucial for ensuring the efficacy of the adsorption method, selecting the most effective material, and optimizing the adsorption process for treating MS.

3.2.1. Effect of pH, contact time, adsorbate concentration, adsorbent dosage

The impact of pH on the AgZnONPs based MS degrading efficiency is depicted in Figure 8(a). The pH range of 3 - 10 was evaluated at a constant adsorbent concentration of 0.5 g/L. At pH 7, the removal efficiency reached a maximum of 92%, representing a considerable increase from 50% at pH 3, indicating that melanoidin adsorption improved under near-neutral conditions [38]. Figure 8(b) shows a diagram of the melanoidin removal efficiency as a function of contact time, with a constant adsorbent concentration of 0.5 g/L. The contact time was varied from 10 min to 120 min. The figure shows that when the contact duration was extended from 10 to 90 minutes, the melanoidin removal efficiency increased quickly from 40% to 92%. After 90 minutes, equilibrium was reached, and the highest color removal efficiency was 92% [39]. Similarly, Figure 9(a) shows how the concentration of melanoidin affects the AgZnONPs ability to absorb. The range of melanoidin values was 50 - 500 mg/L. The 45 mg/g of adsorption capacity at 50 mg/L was elevated to

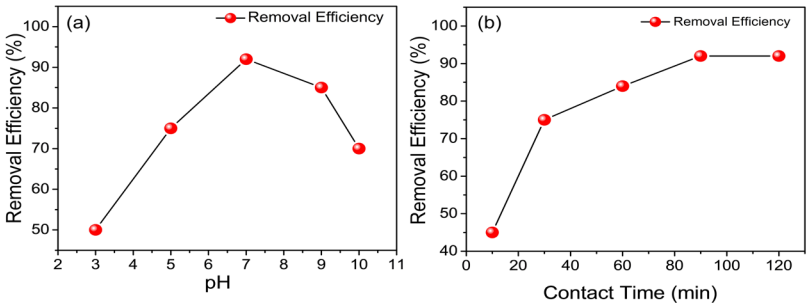

Fig. 8. Adsorption performance analysis: (a) effect of pH on melanoidin removal and (b) effect of contact time on melanoidin removal.

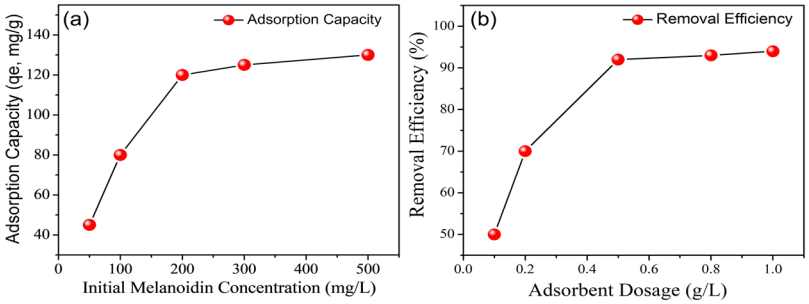

Fig. 9. Adsorption performance analysis: (a) initial melanoidin concentration effect on adsorption capacity and (b) adsorbent dosage effect on melanoidin removal efficiency.

120 mg/g at a concentration of 200 mg/L. When the concentration exceeded 200 mg/L, the adsorption capacity steadily increased to 130 mg/g at 500 mg/L [40]. Figure 9(b) demonstrates the dosage effect on the remediation of MS. The result indicates that the remediation efficacy increases from 50% to 92% if the dosage of AgZnONPs is increased from 0.1 g/L to 0.5 g/L. The consequent pattern is ascribed to the expanded accessibility of active adsorption sites with a maximum adsorbent concentration, resulting in improved pollutant removal until the sites approach saturation [41]. After the dosage was raised over 0.5 g/L, only marginal changes were observed, ranging from 93% to 94% for dosages of 0.8 g/L to 1 g/L.

3.3. Isothermal Analysis

The adsorption isotherms after treatment with MS were studied to evaluate the basic understanding and optimize the sorption process of AgZnONPs. The isothermal models, which were tested using the Langmuir isotherm and Freundlich isotherm are exhibited in Figure 10(a) and Figure 10(b), respectively. The values of the correlation coefficients were in the high range for the Langmuir model ($R^2 = 0.995$) and low range for the Freundlich model ($R^2 = 0.982$). There are no interactions between adsorbed molecules in the Langmuir model, which is a single-layer homogeneous adsorption model. In contrast, the Freundlich model describes multilayered and heterogeneous adsorption phenomena. An excellent fit is provided by the Langmuir model for melanoidin adsorption on the AgZnONPs surface [42]. The specific constant values for both models are listed in Table 1.

3.4. Kinetics Analysis

Adsorption kinetics were evaluated using practical data after treating MS with AgZnONPs to obtain basic information on the rate, mechanism, and efficiency of pollutant removal during the adsorption process. The pseudo-second-order and pseudo-first-order kinetic models are displayed in Figure 11(a) and 10(b), respectively. The kinetic results presented in Table 2 show that the pseudo-second-order kinetic model had a better coefficient

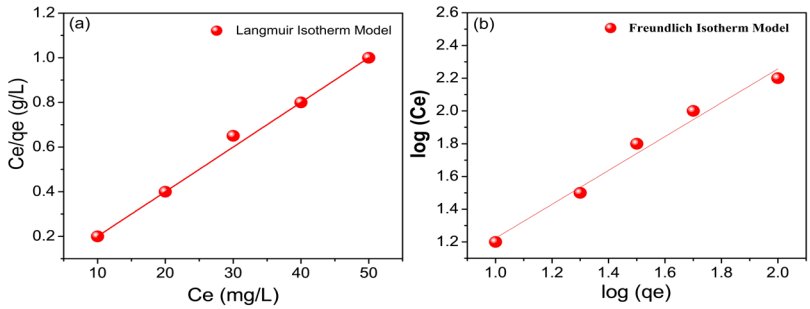

Fig. 10. Adsorption isotherm analysis: (a) Langmuir isotherm model and (b) Freundlich isotherm model.

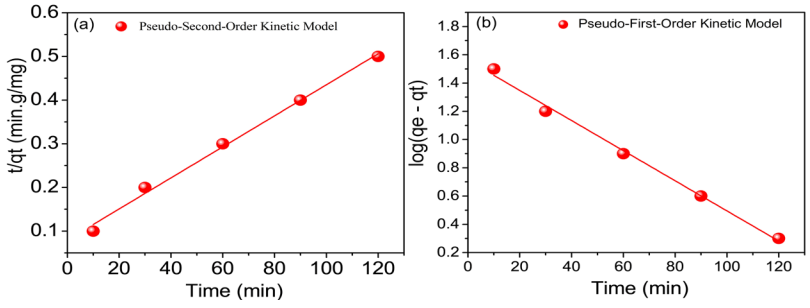

Fig. 11. Adsorption kinetics analysis: (a) pseudo second-order kinetic model and (b) pseudo first-order kinetic model.

Table 1. Linear equations of isotherm models and their constants.

Isotherm models	Linear form	Plots	Constants
Langmuir	$\frac{C_e}{q_e} = \frac{C_e}{q_m} + \frac{1}{K_l q_m}$	$\frac{C_e}{q_e} Vs\ C_e$	q_m = 50mg/g R^2= 0.995
Freundlich	$\log q_e = \log K_f + \left(\frac{1}{n}\right) log C_e$	$log q_e Vs \log C_e$	n=1 R^2=0.982

Table 2. Linear form of Kinetic models and the values of their constants.

Kinetic models	Linear form	Plots	Constants
Pseudo-first order	$\log(q_e - q_t) = logq_e - (K_1/2.303)t$	$\log(q_e - q_t)\ vs\ t$	$k_1 = 0.010$ $R^2 = 0.988$
Pseudo-second order	$\frac{t}{q_t} = \left(\frac{1}{K_2 q_e^2}\right) + (\frac{t}{q_e})$	$\frac{t}{q_t} vs\ t$	$K_2 = 0.00018$ $R^2 = 0.994$

value (R^2 = 0.994) than the pseudo-first-order kinetic model (R^2 = 0.988). Figure 11(a) shows that chemisorption is the speed-limiting step, and this adaptation suggests that chemical interactions between melanoidin and AgZnONPs dominate the adsorption process. The kinetic results indicated that the pseudo-second-order model was more favorable than the pseudo-first-order model for this process [43].

3.5. Melanoidin Removal by AgZnONPs

The AgZnONP-based removal of melanoidin was quantified by changes in the UV-Visible spectrum, as shown in Figure 12. The untreated MS exhibited a prominent absorbance peak at 291 nm, which can be ascribed to the presence of conjugated systems and aromatic moieties capable of absorbing light within the 200–400 nm range [44]. The absorbance at this π→π* wavelength is primarily associated with electronic transitions involving C=C and C=O bonds linked to the aromatic structures [45]. A clear decrease in absorbance intensity was observed after adsorption treatment, suggesting that melanoidin and the adsorbent material interacted well. The

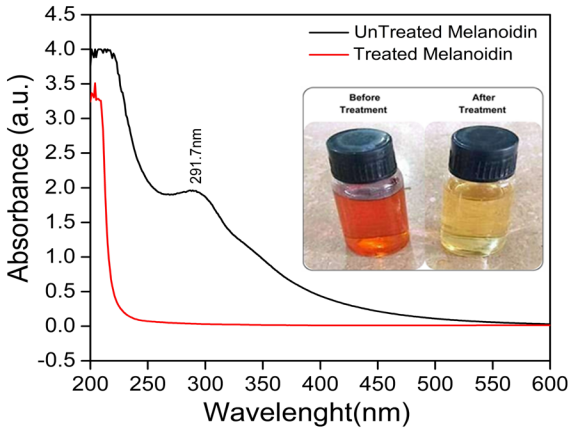

Fig. 12. UV-Visible analysis of untreated and treated MS using AgZnONPs.(Inset: Photographic comparison of MS before and after treatment with AgZnONPs).

results indicate that AgZnONPs treatment of MS results in chromophoric groups in the solution, which leads surface complexation, hydrogen bonding, and electrostatic attraction to cause melanoidin to engage with the nanoparticles, resulting in the reduction of larger aggregates of melanoidin into smaller fragments with distinct UV absorption properties [46-48]. The changes can also be seen through a pictorial comparison of before and after treatment with MS. The inset of Figure 11 clearly shows the color change from dark brown to light yellow for concentrated MS.

3.6. Comparison with other adsorbents

To approximate the interpretation of the as-synthesized AgZnONPs with other reported adsorbents such as activated carbon, Fe-impregnated activated carbon, and oxides of metals for the removal of MS, a comparative assessment is demonstrated in Table 3. These results clearly shows that nanomaterials such as graphene oxide nanosheets exhibited significantly increased theoretical adsorption capacities, with a value of 18,310 mg/g. Although the values are promising, it is essential to note that this performance was accomplished under highly acidic conditions, with a pH of 2, which poses multiple challenges for practical applications. Activated carbon is highly effective, as demonstrated by the 85.6 percent removal efficacy of melanoidin; however, it has several drawbacks, including waste generation, limited reusability, high cost, and sustainability concerns. Similarly, the TiO_2-ZnO composite showed an 86% removal rate; however, using metal oxides as composites makes them costly and limited for large-scale industrial applications. Unlike conventional adsorbents, AgZnONPs overcome these limitations through nanoscale dispersion and the presence of Ag^+ ions, which increase the pollutant binding affinity and electron transmission. Finally, this study exhibits a tantalizing blend with

Table 3. Comparison of adsorbents from previous literature studies.

S. No.	Adsorbent	Max. Adsorption Capacity (mg/g)	Removal Efficiency (%)	Optimal pH	Contact Time (min)	Reference
1	Graphene Oxide Nanosheets	18,310	-	2	120	[49]
2	Chitin Nanofibers	131	-	-	-	[50]
3	Fe-impregnated Activated Carbon	-	85.6	-	75	[51]
4	Coal Fly Ash	281.34	84	6	120	[52]
5	Mesoporous Activated Carbon	23.71	-	-	-	[53]
6	TiO_2-ZnO/AC Composite	-	86	-	-	[54]
7	AgZnONPs	50	92	7	90	This Study

a high removal efficiency (92%) and a respectable adsorption capacity (130 mg/g) under a neutral pH of 7. This functional advantage distinguishes AgZnONPs from other conventional and advanced adsorbents, making them promising nano-material for distillery wastewater treatment.

4. CONCLUSIONS

In summary, AgZnONPs were successfully synthesized using a cost-effective solution process and efficiently used for the adsorption-based removal of MS. The synthesized AgZnONPs were examined using FESEM, XRD, UV-VIS spectroscopy, and FTIR spectroscopy. The structural properties of AgZnONPs were confirmed along with the confirmation of the doping of Ag in ZnO nanoparticles. In addition, MS was treated with AgZnONPs, which resulted in a clear light-yellow solution. UV-Vis absorption spectroscopy confirmed the removal of melanoidin from the treated MS. The AgZnONP-based treatment resulted in an extraordinary adsorption capacity with a maximum removal efficiency of 92%, the best pH value of the treated solution was 7, the initial melanoidin concentration was 200 mg/L for maximum removal efficiency, and the adsorbent dosage of AgZnONPs was 0.5 g/L. In addition, the adsorption performance confirmed that the Langmuir isotherm and pseudo second-order kinetics were feasible and that single-layered sorption and chemisorption mechanisms were feasible. These results highlight the potential of AgZnONPs for the treatment of MS in industrial-scale operations. In order to increase the practical application of AgZnONPs and make it possible for their industrial use to treat distillery effluent, future research should concentrate on their regeneration and reusability.

5. ACKNOWLEDGEMENTS

This study was financially supported by the Higher Education Commission of Pakistan through its National Research Program for Universities (NRPU-7617,2017) and a Deans Research Grant from the Dean of Science and Engineering at the University of Karachi.

6. CONFLICT OF INTEREST

The authors declare no conflict of interest.

7. REFERENCES

1. J.C.-T. Lin, Y.-S. Liu, and W.-K. Wang. A full-scale study of high-rate anaerobic bioreactors for whiskey distillery wastewater treatment with size fractionation and metagenomic analysis of granular sludge. *Bioresource Technology* 306: 123032 (2020).
2. B. Hu, L. Li, Y. Hu, D. Zhao, Y. Li, M. Yang, A. Jia, S. Chen, B. Li, and X. Zhang. Development of a novel Maillard reaction-based time-temperature indicator for monitoring the fluorescent AGE content in reheated foods. *RSC Advances* 10(18): 10402-10411 (2020).
3. M. Murata. Browning and pigmentation in food through the Maillard reaction. *Glycoconjugate Journal* 38(3): 283-294 (2021).
4. S. Tripathi, K. Singh, A.K. Singh, A. Mishra, and R. Chandra. Organo-metallic pollutants of distillery effluent and their toxicity on freshwater fish and germinating Zea mays seeds. *International Journal of Environmental Science and Technology* 19(3): 2021-2036 (2022).
5. M.S.I. Afrad, M.B. Monir, M.E. Haque, A.A. Barau, and M.M. Haque. Impact of industrial effluent on water, soil and rice production in Bangladesh: A

case of Turag River bank. *Journal of Environmental Health Science and Engineering* 18(2): 825-836 (2020).
6. S. Ratna, S. Rastogi, and R. Kumar. Current trends for distillery wastewater management and its emerging applications for sustainable environment. *Journal of Environmental Management* 290: 112544 (2021).
7. R. Patel, R. Gaur, T. Verma, and R. Singh. Challenges of distillery effluent treatment and its bioremediation using microorganism: A review. *Current World Environment* 18(2): 446-459 (2023).
8. L.-N. Ho, S.-A. Ong, S.-H. Thor, and K.-L. Yap. Feasibility of UVA photocatalytic post-treatment of molasses wastewater: Effects on melanoidins removal, mineralization and oxidation of ammoniacal-nitrogen. *Chemical Engineering and Processing: Process Intensification* 196: 109681 (2024).
9. M. Binazadeh, J. Rasouli, S. Sabbaghi, S.M. Mousavi, S.A. Hashemi, and C.W. Lai. An overview of photocatalytic membrane degradation development. *Materials* 16(9): 3526 (2023).
10. Y. Li, Q. Zhang, S. Xiao, Q. Yang, L. Wang, and J. Hao. Review of melanoidins as by-product from thermal hydrolysis of sludge: Properties, hazards, and removal. *Processes* 12(1): 135 (2024).
11. L. Kheddo, L. Rhyman, M.I. Elzagheid, P. Jeetah, and P. Ramasami. Adsorption of synthetic dyed wastewater using activated carbon from rice husk. *SN Applied Sciences* 2(12): 2170 (2020).
12. J. Naser, Z. Ahmed, and E. Ali. Nanomaterials usage as adsorbents for the pollutants removal from wastewater: A review. *Materials Today: Proceedings* 42(5): 2590-2596 (2021).
13. V.S. Kadam, S.S. Wagh, C.V. Jagtap, S.M. Sutar, and R. Mane. Comparative studies on synthesis and photocatalytic activity of ZnO nanoparticles. *ACS Omega* 8(9): 7779-7790 (2023).
14. A. Abdelfattah and A. El-Shamy. A comparative study for optimizing photocatalytic activity of TiO_2-based composites with ZrO_2, ZnO, Ta_2O_5, SnO, Fe_2O_3, and CuO additives. *Scientific Reports* 14(1): 1 (2024).
15. U. Alalawi, U. Romman, K.M. Saleh, S.T. Shafa, and M.U. Khalid. Ag-doped MnO_2 nanowires integrated with graphitic carbon nitride for enhanced photocatalytic applications for wastewater treatment. *Current Applied Physics* 60: 32-39 (2024).
16. W. Xie, B. Li, X. Wu, D. Han, and Y. Zhang. Surface modification of ZnO with Ag improves its photocatalytic efficiency and photostability. *Journal of Photochemistry and Photobiology A: Chemistry* 215: 53-58 (2010).
17. S.K. Noukelag, L.C. Razanamahandry, S.K.O. Ntwampe, C.J. Arendse, and M. Maaza. Industrial dye removal using bio-synthesized Ag-doped ZnO nanoparticles. *Environmental Nanotechnology, Monitoring & Management* 16: 100463 (2021).
18. M. Nandasana, R. Kamat, R. Mishra, P. Ghosh, and S. Patil. Green synthesis of silver and copper-doped zinc oxide nanoflowers for photocatalytic and antibacterial applications. *Vacuum* 212: 111130 (2025).
19. S. Nagasundari, K. Muthu, K. Kaviyarasu, A. Farraj, and R.M. Alkufeidy. Current trends of silver-doped zinc oxide nanowires photocatalytic degradation for energy and environmental application. *Journal of Environmental Chemical Engineering* 23: 100931 (2021).
20. K. Watcharenwong, A. Kongka, C. Kaeokan, C. Chokejaroenrat, and C. Sakulthaew. Decolorization of melanoidin using sonoFenton and photoFenton processes. *Waste* 1(2): 455-467 (2023).
21. K. Brudzynski and D. Miotto. The recognition of high molecular weight melanoidins as the main components responsible for radical-scavenging capacity of unheated and heat-treated Canadian honeys. *Food Chemistry* 125(2): 570-575 (2011).
22. A.L. Jembere and M.B. Genet. Comparative adsorptive performance of adsorbents developed from sugar industrial wastes for the removal of melanoidin pigment from molasses distillery spent wash. *Water Resources and Industry* 26: 100165 (2021).
23. E.D. Revellame, D.L.B. Fortela, W. Sharp, R. Hernandez, and M.E. Zappi. Adsorption kinetic modeling using pseudo-first order and pseudo-second order rate laws: A review. *Cleaner Engineering and Technology* 1: 100032 (2020).
24. M.H. Rahman, M. Marufuzzaman, M.A. Rahman, and M.I.H. Mondal. Adsorption kinetics and mechanisms of nano chitosan coated cotton fiber for the removal of heavy metals from industrial effluents. Heliyon 11(1): e42932 (2025).
25. J.H. Mahamud, A.B. Gemta, A.K. Hordofa, G.A. Argaw, U. Sherefedin, M. Ahmed, T.F. Hurrisa, and T. Gurumurthi. Green synthesis and characterization of silver-doped ZnO nanoparticles using tobacco leaf extract: A novel hydrothermal approach for antibacterial and antifungal applications. *AIP Advances* 15(4): 045030 (2025).
26. S. Hussain, A. Fiaz, A. Almohammedi, and A. Waqar. Optimizing photocatalytic performance

with Ag-doped ZnO nanoparticles: Synthesis and characterization. *Heliyon* 10(15): e35725 (2024).

27. O.A. Zelekew, S.G. Aragaw, F.K. Sabir, D.M. Andoshe, A.D. Duma, D.-H. Kuo, X. Chen, T.D. Desissa, B.B. Tesfamariam, G.B. Feyisa, H. Abdullah, E.T. Bekele, and F.G. Aga. Green synthesis of Co-doped ZnO via the accumulation of cobalt ion onto Eichhornia crassipes plant tissue and the photocatalytic degradation efficiency under visible light. *Materials Research Express* 8(2): 025010 (2021).
28. K. Raza, A. Sayeed, M. Naaz, M. Muaz, S. Rahaman, F. Sama, K. Pandey, and A. Ahmad. Green synthesis of ZnO nanoparticles and Ag-doped ZnO nanocomposite utilizing Sansevieria trifasciata for high-performance asymmetric supercapacitors. *ACS Omega* 9(30): 32444-32458 (2024).
29. M. Karimi-Nazarabad and E. Goharshadi. Ag and Ni doped graphitic carbon nitride coated on wood as a highly porous and efficient photo absorber in interfacial solar steam generation. *Journal of Porous Materials* 30(6): 1835-1845 (2023).
30. R. Radičić, D. Maletić, D. Blažeka, J. Car, and N. Krstulović. Synthesis of silver, gold, and platinum doped zinc oxide nanoparticles by pulsed laser ablation in water. *Nanomaterials* 12(19): 3484 (2022).
31. Z.N. Kayani, F. Manzoor, A. Zafar, M. Mahmood, M. Rasheed, and M. Anwar. Impact of Ag doping on structural, optical, morphological, and photoluminescent properties of ZnO nanoparticles. *Optical and Quantum Electronics* 52(7): 344 (2020).
32. M.B. Islam, M.J. Haque, N.M. Shehab, and M.S. Rahman. Synthesis and characterization (optical and antibacterial) of Ag-doped ZnO nanoparticles. *Open Ceramics* 14: 100370 (2023).
33. N. Ahmed, Z. Khalil, Z. Farooq, K.-U. Haq, S. Shahid, R. Ramiza, P. Ahmad, K.W. Qadir, R. Khan, and Q. Zafar. Structural, optical, and magnetic properties of pure and NiFe-codoped zinc oxide nanoparticles synthesized by a sol-gel autocombustion method. *ACS Omega* 9(1): 137-148 (2023).
34. N. Sedky, A. Afify, A. Almohammedi, E.M.M. Ibrahim, and A.M. Ali. Structural, optical, photoluminescence and magnetic investigation of doped and co-doped ZnO nanoparticles. *Optical and Quantum Electronics* 55: 456 (2023).
35. M. Busilă, V. Mușat, P. Alexandru, C. Romanitan, O. Brîncoveanu, V. Tucureăneanu, I. Mihalache, A.-V. Iancu, and V. Dediu. Antibacterial and photocatalytic activity of ZnO/Au and ZnO/Ag nanocomposites. *International Journal of Molecular Sciences* 24(23): 16939 (2023).
36. T.M. Irine and A. Rathika. Synthesis of silver (Ag) doped zinc oxide nanoparticles as efficient photocatalytic activity for degradation of methylene blue dye. *Journal of Advanced Scientific Research* 13(2): 129-134 (2022).
37. M.A. Kareem, I. Bello, H. Shittu, and P. Sivaprakash. Synthesis, characterization, and photocatalytic application of silver doped zinc oxide nanoparticles. *Cleaner Materials* 3: 100041 (2022).
38. L. Ashwini, L. Saravanan, M. Sabari, M. Astalakshmi, and N. Kanagathara. Effect of Cu doping with varying pH on photocatalytic activity of ZnO nanoparticles for the removal of organic pollutants. *Inorganic Chemistry Communications* 155: 111137 (2023).
39. N. Medoiuni, C. Guillard, F. Dappozze, L. Khrouz, S. Parola, C. Colbeau-Justin, A.B.H. Amara, H.B. Rhaiem, N. Jaffrezic-Renault, and P. Namour. Impact of structural defects on the photocatalytic properties of ZnO. *Journal of Hazardous Materials Advances* 6: 100081 (2022).
40. K. Akpomie and J. Conradie. Synthesis, characterization, and regeneration of an inorganic-organic nanocomposite (ZnO@biomass) and its application in the capture of cationic dye. *Scientific Reports* 10(1): 14441 (2020).
41. S. Rizvi, A. Singh, and S.K. Gupta. A parametric study using Box-Behnken design for melanoidin removal via Cu-impregnated activated carbon prepared from waste leaves biomass. *Applied Water Science* 12(4): 81 (2022).
42. R. Syaifuddin, R. Wahdah, A. Abdullah, and A.R. Saidy. Sorption of phosphate onto surfactant-modified zeolite particles. International Journal of Sciences: *Basic and Applied Research* 61(1): 87-96 (2022).
43. L.Q. Vo, A.-T. Vu, T.D. Le, C.D. Huynh, and H.V. Tran. Fe_3O_4/graphene oxide/chitosan nanocomposite: A smart nanosorbent for lead(II) ion removal from contaminated water. *ACS Omega* 9(15): 17506-17517 (2024).
44. S. Singh, S. Nimse, D.E. Mathew, A. Dhimmar, H. Sahastrabudhe, A. Gajjar, V. Ghadge, P. Kumar, and P.B. Shinde. Microbial melanin: Recent advances in biosynthesis, extraction, characterization, and applications. *Biotechnology Advances* 53: 107773 (2021).
45. X. Huang, W. Ye, J. Zhuang, C. Hu, H. Dong, B. Lei, and Y. Liu. π-Conjugated structure enhances the UV absorption performance of carbon dots and

application in the design of light-colored sunglasses. *ACS Sustainable Chemistry & Engineering* 12(28): 10399-10408 (2024).

46. M. Han, H. Zhao, Z. Liu, J. Liu, X. Li, F. Hang, K. Li, and C. Xie. Color development characteristic and kinetic modeling of Maillard reaction in membrane-clarified sugarcane juice during vacuum evaporation process. *Foods* 14(12): 2136 (2025).
47. B.-H. Fan, Y.-S. Xiong, M.-X. Li, R. Jia, L.-S. Zhou, J.-Y. Tang, W. Li, Y.-W. Lan, H.-Q. Lu, and K. Li. Effective melanoidin adsorption of polyethyleneimine-functionalised molasses-based porous carbon: Adsorption behaviours and microscopic mechanisms. *Separation and Purification Technology* 310: 123016 (2022).
48. I. Šarić and I. Despotović. Hydrogen bonds as stability-controlling elements of spherical aggregates of ZnO nanoparticles: A joint experimental and theoretical approach. *Materials* 16(13): 4843 (2023).
49. S.M. Rafigh and A.R. Soleymani. Melanoidin removal from molasses wastewater using graphene oxide nanosheets. *Separation Science and Technology* 55(13): 2281-2293 (2020).
50. R. Dolphen and P. Thiravetyan. Adsorption of melanoidins by chitin nanofibers. *Chemical Engineering Journal* 166(3): 890-895 (2011).
51. S. Rizvi, L. Goswami, and S.K. Gupta. A holistic approach for melanoidin removal via Fe-impregnated activated carbon prepared from Mangifera indica leaves biomass. *Bioresource Technology Reports* 12: 100591 (2020).
52. S. Ahmed, I.N. Unar, H.A. Khan, G. Maitlo, R.B. Mahar, A.S. Jatoi, A.Q. Memon, and A.K. Shah. Experimental study and dynamic simulation of melanoidin adsorption from distillery effluent. *Environmental Science and Pollution Research* 27: 9619-9636 (2020).
53. K. Suwannahong, S. Wongcharee, J. Rioyo, C. Sirilamduan, and T. Kreetachart. Insight into molecular weight cut-off characteristics and reduction of melanoidin using microporous and mesoporous adsorbent. *Engineering and Applied Science Research* 49(1): 47-57 (2021).
54. B.O. Otieno, S.O. Apollo, B.E. Naidoo, and A. Ochieng. Photodecolorisation of melanoidins in vinasse with illuminated TiO_2-ZnO/activated carbon composite. *Journal of Environmental Science and Health, Part A* 52(7): 616-623 (2017).